Monthly Notices
of the
ROYAL ASTRONOMICAL SOCIETY

Mon. Not. R. Astron. Soc. **419,** 2089–2094 (2012) doi:10.1111/j.1365-2966.2011.19861.x

Suzaku X-ray spectral study of the Compton-thick Seyfert galaxy NGC 5135

Veeresh Singh,[1,2★] Guido Risaliti,[3,4] Valentina Braito[5] and Prajval Shastri[1]

[1]*Indian Institute of Astrophysics, Bangalore 560034, India*
[2]*Department of Physics, University of Calicut, Calicut 673635, India*
[3]*INAF-Osservatorio di Arcetri, Largo E. Fermi 5, I-50125 Firenze, Italy*
[4]*Harvard-Smithsonian Center for Astrophysics, 60 Garden Street Cambridge, MA 02138, USA*
[5]*Department of Physics and Astronomy, University of Leicester, University Road, Leicester LE1 7RH*

Accepted 2011 September 20. Received 2011 September 20; in original form 2011 April 14

ABSTRACT

We present the 0.5–50 keV *Suzaku* broad-band X-ray spectral study of the Compton-thick active galactic nucleus (AGN) in NGC 5135. The *Suzaku* observation provides the first detection of NGC 5135 above 10 keV that allowed us, for the first time, to estimate the absorbing column density, the intrinsic X-ray luminosity, the strength of the reflection component and the viewing angle of the torus for this AGN. The 0.5–10 keV spectrum of NGC 5135 is characterized by the standard components for a Compton-thick source: a scattered continuum, a prominent Fe Kα emission line [equivalent width (EW) $\sim$ 2.1 keV] and a soft excess. At higher energies ($E > 10$ keV), the intrinsic AGN continuum shows up, implying an absorbing column density of the order of $\sim 2.5 \times 10^{24}$ cm^{-2} and the intrinsic 2.0–10 keV X-ray luminosity of $\sim 1.8 \times 10^{43}$ erg s^{-1}. Assuming a toroidal geometry of the reprocessing material, we show that an edge-on view of the obscuring torus is preferred in this source.

Key words: galaxies: active – galaxies: individual: NGC 5135 – galaxies: Seyfert – X-rays: galaxies.

1 INTRODUCTION

Seyfert galaxies host active galactic nuclei (AGNs) powered by accretion on to supermassive black holes. The luminous accreting engine is supposedly surrounded by obscuring material having a torus-like geometry (Antonucci 1993). When the obscuring torus intercepts the observer's line of sight (i.e. type 2 AGNs), the absorbing column density ($N_{\rm H}$) for X-ray photons originating from AGN is typically higher than 10^{22} cm^{-2} (Cappi et al. 2006). In mildly Compton-thick AGNs ($N_{\rm H} \sim$ a few times of 10^{24} cm^{-2}), the primary emission is strongly suppressed below 10 keV and is seen only above 10 keV, while in heavily Compton-thick AGNs ($N_{\rm H} \geq 10^{25}$ cm^{-2}) the primary emission is strongly depressed even at energies above 10 keV due to Compton down-scattering (Matt et al. 2000). In *Chandra*, *XMM–Newton* and earlier observations sensitive only up to 10 keV, Compton-thick AGNs have been identified only by using diagnostic properties such as high equivalent width (EW) of the Fe Kα line ($\geq$1.0 keV; Bassani et al. (1999)), low flux ratio of hard X-ray (2.0–10.0 keV) to [O III] λ5007 Å line emission (Maiolino et al. 1998), and there are no measurements of the true value of the absorbing column density. There is evidence that obscured AGNs are much more numerous than unobscured AGNs, both in the local Universe and at intermediate to high redshifts (Risaliti, Maiolino & Salvati 1999; Hasinger 2008). In recent years, observations from *INTEGRAL*, *Swift* and *Suzaku* have increased the number of Compton-thick sources detected in hard X-ray (Della Ceca et al. 2008; Tueller et al. 2008; Beckmann et al. 2009; Severgnini et al. 2011). However, the number of Compton-thick sources whose broad-band spectra are analysed in detail is still limited. In this paper, we present the *Suzaku* broad-band X-ray spectral properties of NGC 5135, which is one of the brightest known Compton-thick Seyfert type 2 galaxies, with no previous X-ray observations above 10 keV. NGC 5135 has not been detected above 10 keV by any of the hard X-ray detectors, e.g. *BeppoSAX*-PDS, *Swift*-BAT, *INTEGRAL*-IBIS, other than *Suzaku* HXD-PIN. NGC 5135 is a relatively nearby (redshift $z \simeq 0.014$) galaxy and optically classified as a Seyfert type 2 on the basis of emission-line ratios (Phillips, Charles & Baldwin 1983). Infrared (IR) and ultraviolet (UV) studies have shown that NGC 5135 also contains a powerful compact nuclear starburst (González Delgado et al. 1998; Bedregal et al. 2009). The higher spatial resolution of *Chandra* ($\sim$0.5 arcsec) enables isolation of the AGN and starburst emissions, and has shown that the AGN in NGC 5135 is completely obscured by a column density of $N_{\rm H} \geq 10^{24}$ cm^{-2} (Levenson et al. 2004). The Compton-thick obscuration around the AGN in NGC 5135 is also inferred from *ASCA* observations (Turner et al. 1997). Fukazawa et al. (2011) used the *Suzaku* data and reported the presence of

★E-mail: veeresh@iiap.res.in

a high absorbing column density ($N_{\rm H}$) $\sim 2.0 \times 10^{24}$ cm^{-2} and a strong (EW $\sim$ 1.6 keV) Fe Kα emission line in NGC 5135. The primary aim of Fukazawa et al. (2011) was to study the properties of the Fe K line features and its correlation with the absorbing column density and AGN luminosity for a sample of Seyfert galaxies. In this paper, we discuss the detailed broad-band X-ray spectral analysis of NGC 5135 using the same *Suzaku* data, with the aim of characterizing the reprocessing material around the AGN.

2 OBSERVATIONS AND DATA REDUCTION

Suzaku observed NGC 5135 on 2007 July 3 (observation ID 702005010) with an exposure time of $\sim$52.5 ks. *Suzaku* (Mitsuda et al. 2007) carries four X-ray telescopes (XRTs; Serlemitsos et al. (2007)) with X-ray CCD cameras (XIS) at their focal planes. The XISs are sensitive to the 0.2–12.0 keV energy band with 18 $\times$ 18 arcmin^2 field of view. Of the four XIS CCDs, three (XIS 0, 2 and 3) are front illuminated (FI) and one (XIS1) is back illuminated (BI) (Koyama et al. 2007). There are no observations with XIS2, due to a malfunction in 2006 November. *Suzaku* also has a non-imaging hard X-ray detector (HXD; Takahashi et al. 2007) which has two types of detectors, the PIN and the GSO, which are sensitive to the 10–700 keV energy band.

NGC 5135 was detected by XIS 0, 1, 3 and HXD-PIN. We obtained the XIS and HXD event files and reduced these by following the standard procedure described in the *Suzaku* reduction guide,[1] and using the most recent calibration files. For the low-energy instruments (XISs), the source spectra were extracted from a circular region of 2.4 arcmin radius centred on the source. The background spectra were extracted from two circular regions of 2.2 arcmin radius offset from the source and calibration sources. The XIS response (rmfs) and ancillary response (arfs) files were produced using the ftool tasks *xisrmfgen* and *xissimarfgen*, respectively, and the latest calibration files were used. The spectra of the two front-illuminated CCDs (XIS0 and XIS3) were merged. The net XIS source spectra were binned to have a minimum signal-to-noise ratio (S/N) of 4 in each energy bin and χ^2 statistics has been used. For the HXD-PIN, we used the rev2 data that include all four cluster units and the best available background (Fukazawa et al. 2009), which accounts for the instrumental background (NXB; Takahashi et al. 2007) with systematic uncertainties of $\sim$1.3 per cent (at 1σ). We then simulated a spectrum for the cosmic X-ray background counts and added it to the instrumental one. Using this background, NGC 5135 is detected in the 13–50 keV band at $\sim$7 per cent above the background with a net count rate of $(2.7 \pm 0.2) \times 10^{-2}$ cts s^{-1} (a total of $\sim$1400 net source counts have been collected), corresponding to an S/N of $\sim$9.2. Since the HXD-PIN is a non-imaging detector and has a large field of view ($\sim 0.56 \times 0.56$ deg^2), we checked that the HXD-PIN detection of NGC 5135 is not caused and/or contaminated by any other source. In order to do this, we searched the High Energy Astrophysics Science Archive Research Center (HEASARC) and NASA/IPAC Extragalactic Database (NED) for the potential hard X-ray ($E > 10$ keV) emitting sources in a circular region of the radius of 17 arcmin around NGC 5135. The *Swift*, *INTEGRAL* and *BeppoSAX* catalogues do not report any hard X-ray source detection in this area. The *Chandra* and *ASCA* master catalogues report only NGC 5135 as the potential hard X-ray-emitting source. During the *Suzaku* observations, NGC 5135 was placed at the HXD nominal pointing; therefore, in the spectral analysis, we used a cross-calibration constant of 1.18 between the HXD and XIS spectra, as suggested by the *Suzaku*-HXD calibration team.

[1] Available from http://heasarc.gsfc.nasa.gov/docs/suzaku/analysis/abc/

3 *SUZAKU* X-RAY SPECTRAL FIT

The 2.0–10 keV *Suzaku* data can be fitted with a flat power law ($\Gamma \sim$ 1.4) and a Gaussian for the Fe Kα line of high EW ($\sim$3.0 keV), which is broadly similar to the fit reported by previous *Chandra* observations (Levenson et al. 2004). The flat power law and high EW of the Fe Kα line are indicative of the heavily obscured AGN. In order to characterize the X-ray emission from heavily absorbed AGNs, we attempt to fit the 0.5–50 keV *Suzaku* data using physically motivated models.

In order to avoid the complexity of the soft component ($E <$ 2.0 keV), we first attempted to fit the 2.0–50 keV spectrum with a basic model of obscured AGNs, i.e. an absorbed power law representing the AGN X-ray emission transmitted through a cold absorber and an unabsorbed power law for the scattered component. This simple model gives χ^2/degrees of freedom (d.o.f.) $\sim$ 182/31 and leaves large residuals around 6.4 keV with an emission-line-like shape. Adding a Gaussian profile for the Fe Kα at 6.4 keV improves the fit very significantly and gives the fit statistics χ^2/d.o.f. $\sim$ 39/29, with $N_{\rm H} \sim 2.5 \times 10^{24}$ cm^{-2}, $\Gamma \sim 1.8$ for the absorbed component, a steep power law ($\Gamma \sim 2.7$) accounting for the emission below 10 keV and the EW of the Fe Kα line $\sim$2.1 keV. The Fe Kα line is fitted with a narrow Gaussian (σ fixed to 10 eV) and any increase in the linewidth worsens the fit. There are no signatures for the Fe Kβ or the ionized component of Fe Kα line emission in the residuals and the addition of any Gaussian component for such lines worsens the fit statistics. If the photon index (Γ) of the unabsorbed power-law component is fixed to the value equal to the photon index of the absorbed power-law component, the fit statistics does not improve and this fit results $\Gamma \sim 2.1$ with little increase in the column density ($N_{\rm H} \sim 2.6 \times 10^{24}$ cm^{-2}), while the other parameters remain nearly unchanged. Considering the high $N_{\rm H}$ of the absorbed component and the high EW of the Fe Kα line as the indication of the presence of the reflection component, we added the `PEXRAV` (Magdziarz & Zdziarski 1995) model component which represents the emission reflected from a neutral medium. The addition of the reflection component gives χ^2/d.o.f. $\sim$ 33/28 (model 'M1' in Table 1), i.e. an improvement of $\Delta\chi^2 \sim 6$ for 1 d.o.f. at the significance level of 90 per cent. The photon index of the reflected component (`PEXRAV`) was fixed equal to the transmitted component and the reflection scaling factor was fixed to -1, while all other parameters of the `PEXRAV` model were kept to their default values. We note that an equally good fit is obtained if we fix the photon index of the intrinsic power law to 1.9, the canonical value for Seyfert galaxies (Nandra & Pounds 1994). However, as expected, a higher value of the absorbing column density ($N_{\rm H} \sim 2.9 \times 10^{24}$ cm^{-2}) is required to account for the steeper power law. In order to assess the importance of the reflection component, we estimated the 2.0–10 keV X-ray fluxes associated with the unabsorbed power law and the `PEXRAV` (reflection) model components using the model 'M1'. The 2.0–10 keV X-ray fluxes associated with the unabsorbed power law and the `PEXRAV` (reflection) model components are $\sim 1.27 \times 10^{-13}$ erg cm^{-2} s^{-1} and $\sim 1.49 \times 10^{-13}$ erg cm^{-2} s^{-1}, respectively. These flux values correspond to $\sim$28 and $\sim$34 per cent of the total observed flux in the 2.0–10 keV band, respectively, and suggest that both the unabsorbed power law and the reflection components contribute substantially in this band.

Since Compton scattering is significant for large column densities and high-energy photons (Yaqoob 1997), we applied the scattering

Table 1. The best-fitting spectral parameters.

Energy range	Model	Soft component		Hard component			Fe Kα line		χ^2/d.o.f.
		kT (keV)	$\Gamma_{\rm soft}$	$N_{\rm H}$ ($\times10^{24}$ cm^{-2})	$\Gamma_{\rm hard}$	R	$E_{\rm line}$ (keV)	EW$_{\rm Fe}$ (keV)	
2.0–50.0	M5	...	$2.04^{+0.26}_{-0.08}$	$2.71^{+0.81}_{-0.75}$	$1.96^{+0.26}_{-0.08}$	...	...	...	44.9/27
2.0–50.0	M1	...	$2.76^{+0.29}_{-0.25}$	$2.50^{+1.28}_{-0.92}$	$1.50^{+1.05}_{-0.71}$	$0.40^{+0.58}_{-0.27}$	$6.38^{+0.01}_{-0.01}$	$2.01^{+0.44}_{-0.27}$	32.8/28
2.0–50.0	M1†	...	$2.76^{+0.22}_{-0.18}$	$2.51^{+1.06}_{-1.08}$	$1.51^{+1.01}_{-0.66}$	...	$6.38^{+0.01}_{-0.01}$	$2.14^{+0.36}_{-0.38}$	32.6/28
2.0–50.0	M1‡	...	$2.88^{+0.16}_{-0.22}$	$2.33^{+1.03}_{-0.91}$	$1.68^{+0.90}_{-0.71}$	...	$6.38^{+0.01}_{-0.01}$	$2.09^{+0.42}_{-0.38}$	32.5/27
2.0–50.0	M2	...	$2.17^{+0.78}_{-0.52}$	$2.34^{+0.56}_{-0.36}$	$1.64^{+0.28}_{-0.16}$	...	...	...	37.6/28
0.5–50.0	M3	$0.67^{+0.09}_{-0.04}$	$2.73^{+0.19}_{-0.17}$	$2.59^{+1.04}_{-0.68}$	$1.55^{+1.09}_{-0.66}$	$0.42^{+1.64}_{-0.21}$	$6.38^{+0.01}_{-0.01}$	$2.10^{+0.46}_{-0.32}$	89.0/70
0.5–50.0	M3†	$0.73^{+0.07}_{-0.03}$	$2.82^{+0.18}_{-0.18}$	$2.74^{+1.76}_{-1.05}$	$1.59^{+1.02}_{-0.69}$	...	$6.38^{+0.01}_{-0.01}$	$2.07^{+0.44}_{-0.38}$	91.4/70
0.5–50.0	M3‡	$0.67^{+0.08}_{-0.03}$	$2.71^{+0.19}_{-0.18}$	$2.30^{+1.00}_{-0.98}$	$1.60^{+0.97}_{-0.79}$	...	$6.38^{+0.01}_{-0.01}$	$2.09^{+0.40}_{-0.28}$	89.0/70
0.5–50.0	M4	$0.80^{+0.06}_{-0.06}$	$2.31^{+0.12}_{-0.07}$	$2.20^{+0.36}_{-0.27}$	$1.65^{+0.26}_{-0.12}$	...	...	...	107.7/72

Notes. M1: const(pl+wabs*pl+pexrav+line); M1†: const(pl+wabs*cabs*pl+pexrav+line); M1‡: const(pl+plcabs+pexrav+line); M2: const(pl+wabs*pl+reflionx.mod); M3: const(mekal+pl+wabs*pl+pexrav+line); M3†: const(mekal+pl+wabs*cabs*pl+pexrav+line); M3‡: const(mekal+pl+plcabs+pexrav+line); M4: const(mekal+pl+wabs*pl+reflionx.mod); M5: MYTORUS (Murphy & Yaqoob 2009).

component using the CABS model to the primary transmitted component (model 'M1†' in Table 1). However, the CABS model does not account for the photons scattered into the line of sight from other directions. To account for this effect, we fitted the spectrum with a model ('M1‡' in Table 1) in which the PLCAB model accounts for Compton scattering assuming a uniform, spherically distributed reprocessing material around the X-ray-emitting source (Yaqoob 1997). This model also gives fit statistics (χ^2/d.o.f. $\sim$ 32.5/27) and parameters similar to models 'M1' and 'M1†' (cf. Table 1).

We also checked the spectral fitting with a model ('M2' in Table 1) in which the reflection component is accounted by the REFLIONX model (Ross & Fabian 2005). The REFLIONX model characterizes the reflected emission from an optically thick disc illuminated by radiation with a power-law spectrum and produces the florescent emission lines as well as the continuum emission. The best fit which could fit the Fe Kα emission line gives unusually high Fe abundance ($\sim$10 times solar), a low-ionization parameter ($\xi \sim 91^{+160}_{-78}$ erg cm s^{-1}) and a photon index (Γ) of $\sim$1.6 with χ^2/d.o.f. $\sim$ 37.6/28. The required high abundance and the low-ionization parameter suggest that the Fe line emission originates mainly from the neutral or mildly ionized material.

Since the PLCAB model is valid up to energies between 10 and 18.5 keV and for column densities up to $\sim5 \times 10^{24}$ cm^{-2} (Yaqoob 1997), we attempted to use the MYTORUS model (Murphy & Yaqoob 2009), which accounts for the photoelectric absorption, Compton down scattering as well as Fe Kα, Kβ line emission and is valid for the 0.5–500 keV energy band and for a column density of up to 10^{25} cm^{-2}. This model considers an azimuthally symmetric toroidal geometry around AGNs for the X-ray reprocessor and produces the reprocessed continuum and Fe Kα, Fe Kβ lines self-consistently. The opening angle of the torus is fixed to 60° and the column density and the viewing angle are free parameters. The best fit using the MYTORUS model ('M5') renders $N_{\rm H} \sim 2.7 \times 10^{24}$ cm^{-2}, $\Gamma \sim 1.96$, and the viewing angle of the torus $\sim$90°, with χ^2/d.o.f. $\sim$ 45/27. The best fit is obtained by fixing the viewing angle to 90°. If we allow it to vary, the fit statistics does not improve (i.e. a similar χ^2 value with decrease of 1 in d.o.f.) and gives a viewing angle of $\geq$88° at the 90 per cent confidence level. We note that while using the MYTORUS model ('M5'), an additional unabsorbed power law of a photon index $\sim$2.0 is required to fit the data below 10 keV.

We finally fitted the whole 0.5–50 keV spectrum with the above models and noted that addition of a thermal plasma model (MEKAL in XSPEC) of temperature $kT \sim 0.70$ keV is required to account for the emission below 2.0 keV (models 'M3', 'M3†', 'M3‡' and 'M4' in Table 1). While fitting the 0.5–50 keV spectrum, we have excluded the XIS data points lying in the 1.6–1.9 keV energy range because they are likely to be affected by systematic calibration uncertainties around the instrumental silicon K-edge. We find that the best-fitting parameters obtained are similar in both the 2.0–50 keV and 0.5–50 keV spectral fittings. This implies that the addition or removal of the soft component ($E < 2.0$ keV) does not affect the interpretation of the hard components. Table 1 lists the models and their resulting best-fitting parameters. All the quoted errors are at the 90 per cent confidence level for one interesting parameter. The best-fitting spectrum using model 'M3' and the unfolded model are shown in Fig. 1. Fig. 2 shows the confidence contours for the photon index versus absorbing column density using model 'M3'.

4 DISCUSSION

4.1 Soft X-ray emission

In our *Suzaku* X-ray spectral fitting, the soft X-ray emission below 2.0 keV is accounted by a thermal plasma model of temperature $kT \sim 0.70$ keV and a steep unabsorbed power law. The observed 0.5–2.0 keV luminosity is $\sim1.66 \times 10^{41}$ erg s^{-1} (cf. Table 2), consistent with previous *ASCA* and *Chandra* observations within the measurement uncertainties. The ratio of the soft X-ray to far-IR emission ($L_{0.5-2.0\,\rm keV}/L_{\rm FIR}$) $\sim 3.0 \times 10^{-4}$ for NGC 5135 is consistent with the typical ratio observed in starburst galaxies (e.g. Ranalli, Comastri & Setti 2003), suggesting that the soft X-ray emission is dominated by starburst emission. Indeed, the *Chandra* observation of the high spatial resolution shows that the 0.5–2.0 keV soft X-ray emission from the central region is dominated by the circumnuclear starburst. The soft X-ray spectral components, i.e. thermal component of temperature $kT \sim 0.70$ keV and a steep power law ($\Gamma \sim 2.7$), in our *Suzaku* data are fairly consistent with the X-ray spectral properties of a spatially resolved strong circumnuclear starburst region identified in the *Chandra* observation (Levenson et al. 2004). The steep unabsorbed power law is likely to have contribution from different individual sources, mainly X-ray binaries in the starburst region (Zezas et al. 2002). A high-resolution near-IR study of the central $\sim$2.3 kpc region in NGC 5135 has revealed the star formation knots and a large $\sim$600 pc [Si VI] 1.96-μm line emission ionization

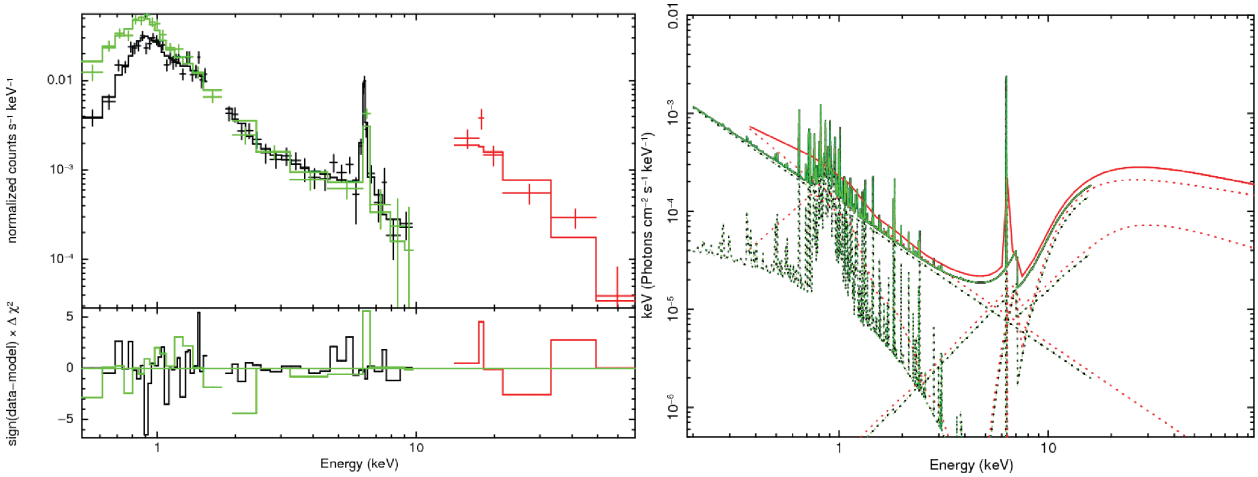

Figure 1. The *Suzaku* 0.5–50 keV spectral fit using model 'M3'. The left-hand panel shows the spectral fit and residuals (in the bottom panel) and the right-hand panel shows the unfolded model 'M3'. The XIS0+3, XIS1 and HXD-PIN data points and spectral components are shown in black, green and red, respectively. In the unfolded model, the additive components are shown by dotted curves and the cumulative model is shown by solid curves.

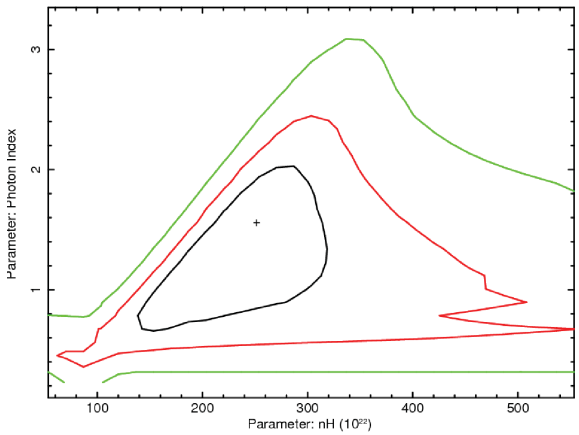

Figure 2. Confidence contours for the photon index versus absorbing column density obtained from model 'M3'. Contours at 1σ, 2σ and 3σ levels are shown in black, red and green, respectively.

Table 2. *Suzaku* X-ray fluxes and luminosities of NGC 5135.

Energy (keV)	Model	$F_{\rm obs}$ (erg cm^{-2} s^{-1})	$L_{\rm obs}$ (erg s^{-1})	$\frac{F_{\rm cor}}{F_{\rm obs}}$
0.5–2.0	M3	3.89×10^{-13}	1.66×10^{41}	5.0
	M3†	3.89×10^{-13}	1.66×10^{41}	65.9
	M3‡	3.89×10^{-13}	1.66×10^{41}	16.6
	M4	3.88×10^{-13}	1.66×10^{41}	12.3
2.0–10	M3	4.44×10^{-13}	1.89×10^{41}	11.3
	M3†	4.40×10^{-13}	1.87×10^{41}	124.8
	M3‡	4.43×10^{-13}	1.89×10^{41}	27.0
	M4	4.37×10^{-13}	1.86×10^{41}	20.5
	M5	4.17×10^{-13}	1.78×10^{41}	135.5
10–50	M3	1.58×10^{-11}	6.67×10^{42}	1.2
	M3†	1.50×10^{-11}	6.39×10^{42}	8.4
	M3‡	1.50×10^{-11}	6.67×10^{42}	1.7
	M4	1.49×10^{-11}	6.35×10^{42}	1.3
	M5	1.46×10^{-11}	6.17×10^{42}	4.5
Fe Kα	M3	9.35×10^{-14}	3.98×10^{40}	...

Notes. $F_{\rm obs}$: observed flux; $L_{\rm obs}$: observed luminosity; $F_{\rm cor}$: absorption-corrected flux.

cone centred on AGNs (Bedregal et al. 2009). It has been argued that supernova remnant shocks play a dominant role in ionizing the gas in the central ∼2.3 kpc region, and photoionized emission due to AGNs and the recent star formation have rather localized and smaller contribution (Bedregal et al. 2009). Note that, in general, high-resolution X-ray grating spectral studies show that the soft X-ray emission in Seyfert 2 galaxies is dominated by recombination lines, implying photoionization as the primary mechanism (Kinkhabwala et al. 2002; Guainazzi & Bianchi 2007; Marinucci et al. 2011). However, the soft X-ray emission in Seyfert 2 galaxies with intense circumnuclear starburst is likely to be dominated by the collisionally ionized optically thin plasma emission associated with star formation (Guainazzi et al. 2009). Limited spatial and spectral resolution of the *Suzaku* XIS CCD does not allow us to quantify the AGN and starburst contribution to the 0.5–2.0 keV soft X-ray emission, which, in turn, does not allow us to draw firm conclusions about the origin of the soft X-ray emission. X-ray observations of high spectral and spatial resolution are required to confirm the nature of the soft X-ray emission in NGC 5135.

4.2 Hard X-ray emission

Our *Suzaku* X-ray spectral fitting shows that the 2.0–10 keV continuum emission has contribution from several spectral components, e.g. steep unabsorbed power law, thermal plasma model, reflection component and absorbed power law (see Fig. 1). However, the relative contribution from each individual spectral component is energy dependent. For example, the relative contribution of the unabsorbed power law decreases towards higher energies, while it increases for the reflection component. The thermal plasma model and absorbed power-law components contribute only to the soft and hard parts of the 2.0–10 keV band, respectively. Using star formation rate (SFR) and X-ray correlation (SFR $\simeq 2.0 \times L_{2.0-10\,\rm keV}\,{\rm M}_{\odot}\,{\rm yr}^{-1}$) from Ranalli et al. (2003) and assuming SFR $\sim 15\ {\rm M}_{\odot}\,{\rm yr}^{-1}$ in NGC 5135 (Bedregal et al. 2009), we noted that the estimated contribution from the circumnuclear starburst to the 2.0–10 keV X-ray luminosity is $\sim 7.5 \times 10^{40}$ erg s^{-1}, which is ∼40 per cent of the total observed 2.0–10 keV luminosity. This value is similar to the 2.0–10 keV non-AGN X-ray luminosity reported in the *Chandra*

observation, which could spatially resolve the AGN and circumnuclear starburst X-ray emission (Levenson et al. 2004). The above argument implies that nearly ∼60 per cent of the total observed 2.0–10 keV X-ray emission is attributed to AGN emission, which is accounted by the scattered, reflected and transmitted components. Our *Suzaku* (0.5–50 keV) broad-band X-ray spectral analysis of NGC 5135 shows the characteristics of starburst as well as obscured AGNs and thus confirming its composite nature. Furthermore, the X-ray emission from circumnuclear starburst regions in NGC 5135 can be characterized by both the thermal plasma model and unabsorbed power law (Levenson et al. 2004). Note that star-forming galaxies show characteristic power-law X-ray emission that could be the integrated spectrum of distinct X-ray sources (Zezas et al. 2002). Moreover, an unabsorbed power-law component representing the scattered emission of the primary AGN continuum to the line of sight is also commonly seen in obscured AGNs (Braito et al. 2009; Comastri et al. 2010; Severgnini et al. 2011). With present *Suzaku* data we cannot spatially separate out the AGN and circumnuclear starburst emission and therefore it is possible that the unabsorbed power-law component in our spectral fitting may have contribution from both the *circumnuclear* starburst and the scattered component of AGN emission. It is likely that the quality of the present 2.0–50 keV *Suzaku* data does not allow us to accurately determine the relative contributions from starburst, scattered, reflected and absorbed AGN emission spectral components in the 2.0–10 keV energy band.

Our *Suzaku* 2.0–50 keV broad-band spectral fitting clearly shows that the hard X-ray continuum is characterized by a heavily absorbed power law and a reflection component, consistent with the previous results reported by Fukazawa et al. (2011). The high absorbing column density ($N_{\rm H} \sim 2.5 \times 10^{24}$ cm^{-2}) and the high ratio of the intrinsic to the observed 2.0–10 keV flux/luminosity (see Table 2) infer the presence of a heavily obscured, luminous AGN. The ratio of the intrinsic to the observed flux/luminosity in the 2.0–10 keV band, found for NGC 5135, is consistent with the typical values observed in other Compton-thick AGNs (Levenson et al. 2006; Brightman & Nandra 2011). Given the importance of Compton scattering in absorbers with column densities of a few times of 10^{24} cm^{-2}, the absorption-corrected (intrinsic) flux/luminosity is model dependent. The value of the intrinsic luminosity ($[(L_{2.0-10\,{\rm keV,int}})/(L_{2.0-10\,{\rm keV,obs}})] \sim 125$) obtained from model 'M3†', which uses the CABS model for the scattering, can be considered as the upper limit. Since the CABS model represents the Compton scattering from the matter only along the line of sight, it offers a small covering fraction, i.e. a single cloud along the line of sight which only removes photons from the beam owing to Compton scattering and does not consider the addition of photons scattered from other directions into the line of sight. Moreover, the ratio of the intrinsic to the observed flux/luminosity also depends on the photon index of the intrinsic power law; for example, this ratio obtained from the M3† model is as high as ∼300, if we fix the photon index to 1.9. The value of the intrinsic luminosity obtained from model 'M3‡', where the PLCABS model is used for scattering, can be considered as a lower limit, since in this scenario, the contribution from photons initially not in the line of sight, which are then scattered to the line of sight, is highest and roughly compensates for the loss of photons that are initially along the line of sight and that are scattered out. Thus, the two models represent two limits: a single cloud covering (CABS) gives an upper limit and full covering (PLCABS) gives a lower limit on the intrinsic luminosity, and the true value lies somewhere in between depending on the covering factor. In the MYTORUS model, the covering factor corresponds to 0.5 and the ratio of the intrinsic to the observed flux/luminosity (∼135) indeed lies between the two limits, if the photon index of the intrinsic power law is assumed to be 1.9.

High obscuration around the AGN is also inferred from the flux ratio of the hard (2.0–10 keV) X-ray to [O III] λ5007 Å line emission (Bassani et al. 1999); i.e. for NGC 5135, we obtain $\log[F_{2.0-10\,{\rm keV,obs}}/F_{[{\rm O\,III}]}] \simeq -1.1$, using the reddening-corrected [O III] flux given in Singh, Shastri & Risaliti (2011). Furthermore, the flux ratio of the intrinsic 2.0–10 keV hard X-ray to [O III] λ5007 Å line emission is ($F_{2.0-10\,{\rm keV,int}}/F_{[{\rm O\,III}]}$) ∼9.2, consistent with the mean ratio observed in Seyfert 1 galaxies (Heckman et al. 2005), supporting the notion that the obscured nucleus in NGC 5135 is intrinsically similar to a Seyfert type 1 nucleus.

The signature of the Compton-thick matter around the AGN can be characterized by Compton reflection continuum with a broad hump peaking around 20–30 keV, which rapidly decreases at both low and high energies due to photoelectric absorption and Compton down-scattering, respectively. In our spectral fits, the reflection strength measured as the ratio of the normalizations of the reflection component to the transmitted component (absorbed power law) is ∼0.4 (using model 'M1'). We do not attempt to compare the strengths of the reflection components obtained by using the MYTORUS and PEXRAV models since these models consider different geometries for the reprocessor. The relative strength of the reflection continuum depends critically on geometry since it is affected by the angle of reflection integrated over the surface of the reprocessor. Murphy & Yaqoob (2009) showed that the reflection spectrum from a Compton-thick face-on torus that subtends the same solid angle as a Compton-thick face-on accretion disc at the X-ray source is much weaker and it is not meaningful to compare the reflection strength given by the MYTORUS model with one from the PEXRAV model.

4.3 Geometry of the absorber

Note that the PEXRAV and REFLIONX models consider reflection from the surface of the accretion disc and are therefore insufficient to constrain the geometry of the toroidal-shaped obscuring material around the AGN. We used the MYTORUS model (Murphy & Yaqoob 2009), which considers the geometry of the reprocessing material as an azimuthally symmetric obscuring torus. This model suggests the edge-on view (i.e. the viewing angle ∼90°) of the obscuring torus. The absorbing column density given by the MYTORUS model corresponds to the equatorial column density of the toroidal-shaped obscuring material. We note that the column densities obtained from the MYTORUS and other models are similar within the uncertainties (see Table 1), confirming again that the obscuring torus is oriented nearly edge-on. We caution that in the current version of the MYTORUS model, the torus opening angle is fixed to 60°, while it needs to be a varying parameter. The opening angle of 60° corresponds to a covering factor of 0.5 and the solid angle subtended by the torus on to the X-ray-emitting source to 2π. Hints on the covering fraction of the absorber, as seen from the X-ray source, can be inferred from our fits. It has been shown that variation in the geometry of the obscuring torus, and not the iron abundance or intrinsic spectral shape, is required to produce EWs significantly larger than 1 keV and therefore the EW of the Fe Kα line can be used to place limits on the covering factor (Levenson et al. 2002). Levenson et al. (2002) argued that the high EW of the Fe Kα line (∼2.1 keV) in NGC 5135 suggests a small opening angle (∼20°) of the obscuring torus giving a covering fraction of ∼90 per cent. Our *Suzaku* X-ray spectral fitting gives $L_{\rm Fe} \simeq 3.98 \times 10^{40}$ erg s^{-1} and using the Levenson et al. (2006) empirical ratio of the Fe Kα line luminosity to the intrinsic 2.0–10 keV luminosity, we obtain

$L_{2-10\,\mathrm{keV,int}} \sim 1.99 \times 10^{43}\,\mathrm{erg\,s^{-1}}$, i.e. nearly 100 times the observed 2.0–10.0 keV luminosity. This value of the 2.0–10 keV intrinsic luminosity lies between the values from the MYTORUS model (a covering fraction of ∼50 per cent) and the M3‡ model that uses the PLCABS model (a covering fraction of ∼100 per cent). Furthermore, we note that the intrinsic 2.0–10 keV X-ray luminosity obtained by using the mid-IR (12 μm)–X-ray luminosity correlation (L_{MIR}–$L_{2.0-10\,\mathrm{keV}}$) and mid-IR luminosity (L_{MIR}) $\sim 1.15 \times 10^{43}\,\mathrm{erg\,s^{-1}}$ given in Gandhi et al. (2009) is $\sim 7.6 \times 10^{42}\,\mathrm{erg\,s^{-1}}$, which again lies between the values from models M5 and M3‡. The high-resolution mid-IR core fluxes/luminosities presented in Gandhi et al. (2009) are reported to be least contaminated by the circumnuclear starburst and primarily represent the emission from the torus. The above comparisons for the 2.0–10 keV intrinsic luminosities suggest that the covering factor lies between 50 and 100 per cent. Finally, the low ratio between the soft power-law flux and the intrinsic emission (<0.01; Table 2) suggests a low scattering efficiency, which again may be due to a high covering factor of the thick absorber, leaving only a small fraction of the solid angle free for the primary continuum to reach the warm scatterer. A similar low flux ratio (<0.01) of the unabsorbed power law to the intrinsic 2.0–10 keV emission is obtained with model 'M5', which considers an axisymmetric toroidal geometry of the reprocessing material around the AGN. The actual scattered fraction may be even lower, given that part of the soft power law may be due to the starburst emission.

5 CONCLUSIONS

We have analysed the *Suzaku* XIS+HXD-PIN observation of the AGN in NGC 5135. We found that the 0.5–50 keV spectrum can be reproduced by a model consisting of (i) a soft component, characterized by a thermal plasma model (the MEKAL) of temperature $kT \sim 0.70$ keV plus an unabsorbed steep power law ($\Gamma \sim 2.7$); (ii) a hard component best fitted by an absorbed power law ($N_{\mathrm{H}} \sim 2.5 \times 10^{24}\,\mathrm{cm^{-2}}$, $\Gamma \sim 1.6$), a reflection continuum component and a prominent Fe Kα line with EW ∼ 2.1 keV. The *Suzaku* broad-band energy coverage allowed us to accurately measure the absorbing column density, intrinsic AGN luminosity and the reflection component. We attempted various physically motivated models and all the models confirm that the AGN in NGC 5135 is obscured by Compton-thick material. The MYTORUS model, which considers the geometry of the reprocessing material as an azimuthally symmetric torus, suggests that the torus is viewed nearly edge-on. Both the estimates on the reflection strength and the comparison between the emission line flux and the continuum flux suggest that the obscuring torus may cover 90 per cent of the line of sight. Our *Suzaku* X-ray spectral study of NGC 5135 may represent a case study of some of the complex features in Compton-thick obscured AGNs.

ACKNOWLEDGMENTS

This research has made use of data obtained from the *Suzaku* satellite, a collaborative mission between the space agencies of Japan (JAXA) and the USA (NASA). The authors also thank the anonymous referee for useful comments that helped to improve the quality of the paper.

REFERENCES

Antonucci R., 1993, ARA&A, 31, 473
Bassani L., Dadina M., Maiolino R., Salvati M., Risaliti G., Della Ceca R., Matt G., Zamorani G., 1999, ApJS, 121, 473
Beckmann V. et al., 2009, A&A, 505, 417
Bedregal A. G., Colina L., Alonso-Herrero A., Arribas S., 2009, ApJ, 698, 1852
Braito V., Reeves J. N., Della Ceca R., Ptak A., Risaliti G., Yaqoob T., 2009, A&A, 504, 53
Brightman M., Nandra K., 2011, MNRAS, 413, 1206
Cappi M. et al., 2006, A&A, 446, 459
Comastri A., Iwasawa K., Gilli R., Vignali C., Ranalli P., Matt G., Fiore F., 2010, ApJ, 717, 787
Della Ceca R. et al., 2008, Mem. Soc. Astron. Ital., 79, 65
Fukazawa Y. et al., 2009, PASJ, 61, 17
Fukazawa Y. et al., 2011, ApJ, 727, 19
Gandhi P., Horst H., Smette A., Hönig S., Comastri A., Gilli R., Vignali C., Duschl W., 2009, A&A, 502, 457
González Delgado R. M., Heckman T., Leitherer C., Meurer G., Krolik J., Witson A. S., Kinney A., Koratkar A., 1998, ApJ, 505, 174
Guainazzi M., Bianchi S., 2007, MNRAS, 374, 1290
Guainazzi M., Risaliti G., Nucita A., Wang J., Bianchi S., Soria R., Zezas A., 2009, A&A, 505, 589
Hasinger G., 2008, A&A, 490, 905
Heckman T. M., Ptak A., Hornschemeier A., Kauffmann G., 2005, ApJ, 634, 161
Kinkhabwala A. et al., 2002, ApJ, 575, 732
Koyama K. et al., 2007, PASJ, 59, 23
Levenson N. A., Krolik J. H., Życki P. T., Heckman T. M., Weaver K. A., Awaki H., Terashima Y., 2002, ApJ, 573, L81
Levenson N. A., Weaver K. A., Heckman T. M., Awaki H., Terashima Y., 2004, ApJ, 602, 135
Levenson N. A., Heckman T. M., Krolik J. H., Weaver K. A., Życki P. T., 2006, ApJ, 648, 111
Magdziarz P., Zdziarski A. A., 1995, MNRAS, 273, 837
Maiolino R., Salvati M., Bassani L., Dadina M., Dalla Ceca R., Matt G., Risaliti G., Zamorani G., 1998, A&A, 338, 781
Marinucci A., Bianchi S., Matt G., Fabian A. C., Iwasawa K., Miniutti G., Piconcelli E., 2011, A&A, 526, A36
Matt G., Fabian A. C., Guainazzi M., Iwasawa K., Bassani L., Malaguti G., 2000, MNRAS, 318, 173
Mitsuda K. et al., 2007, PASJ, 59, 1
Murphy K. D., Yaqoob T., 2009, MNRAS, 397, 1549
Nandra K., Pounds K. A., 1994, MNRAS, 268, 405
Phillips M. M., Charles P. A., Baldwin J. A., 1983, ApJ, 266, 485
Ranalli P., Comastri A., Setti G., 2003, A&A, 399, 39
Risaliti G., Maiolino R., Salvati M., 1999, ApJ, 522, 157
Ross R. R., Fabian A. C., 2005, MNRAS, 358, 211
Serlemitsos P. J. et al., 2007, PASJ, 59, 9
Severgnini P., Caccianiga A., Della Ceca R., Braito V., Vignali C., La Parola V., Moretti A., 2011, A&A, 525, A38
Singh V., Shastri P., Risaliti G., 2011, A&A, 532, A84
Takahashi T. et al., 2007, PASJ, 59, 35
Tueller J., Mushotzky R. F., Barthelmy S., Cannizzo J. K., Gehrels N., Markwardt C. B., Skinner G. K., Winter L. M., 2008, ApJ, 681, 113
Turner T. J., George I. M., Nandra K., Mushotzky R. F., 1997, ApJS, 113, 23
Yaqoob T., 1997, ApJ, 479, 184
Zezas A., Fabbiano G., Rots A. H., Murray S. S., 2002, ApJ, 577, 710

This paper has been typeset from a TEX/LATEX file prepared by the author.